Models for Plasmonic THz Detectors Based on Graphene Split-Gate FETs with Lateral p-n Junctions

Maxim Ryzhii*, Victor Ryzhii†‡, Akira Satou†, Taiichi Otsuji†, Vladimir Mitin§, and Michael S. Shur¶

*Department of Computer Science and Engineering
University of Aizu, Aizu-Wakamatsu, Japan 965-8580
Email: m-ryzhii @ ieee.org
†Institute of Electrical Communications
Tohoku University, Sendai, Japan 980-8577
‡Institute of Ultra High Frequency Semiconductor Electronics
Russian Academy of Ssciences, Moscow 117105, Russia
§Department of Electrical Engineering
University at Buffalo, SUNY, Buffalo, New York 1460-1920, USA
¶Department of Electrical, Computer, and Systems Engineering
Rensselaer Polytechnic Institute, Troy, New York 12180, USA

Abstract—We propose and analyze the resonant plasmonic terahertz detectors based on the split-gate field-effect transistors with electrically induced p-n junctions and graphene and perforated graphene channels. The perforation of the p-n junction depletion region leads to the tunneling suppression and the substantial reinforcement of the detector resonant response.

I. INTRODUCTION

The nonlinearity of the current-voltage characteristics of the lateral p-n-junctions [1], [2], [3], [4] in graphene layers (GLs) can be used for detection of terahertz (THz) radiation using the effect of the current rectification The gated regions of p- and n-types form the plasmonic cavities [5], so that the excitation of the plasmonic oscillations by THz radiation can substantially enhance the detector characteristics due to the plasmonic resonances even at room temperature (for example, [6]). Due to the specific features of the electron properties of GLs, GBL, and GNR structures [5], first of all high carrier mobility at room temperature(about 110,000 cm^2/V s in the epitaxially grown GLs on SIC substrate), these structures can be the building blocks for room temperature plasmonic detectors of THz radiation with the enhanced performance [7].

In this paper, we propose and analyze the resonant THz detector based on split-gate GL-FET and split-gate FET with the GL perforated between the gates (PGL-FET). This perforated region can be considered as an array of the nanoconstrictions or GNRs similar to the GNR channels of FETs [8], [9].

In these GL- and PGL-FETs the GL channel is partitioned into the p- and n-type sections (see also [10]). The operation of such detectors is enabled by the nonlinearity of the p-n-junction and the excitation of coupled plasmonic oscillations in the gated channel sections. The perforation of the GL portion corresponding to the p-n-junction depletion region leads to the formation of an array of nanocostrictions, which,

in turn, create the potential barrier substantially suppressing the interband tunneling in the p-n junction. This results in dramatic enhancement of the detector resonant responsivity.

II. MAIN EQUATIONS

We consider the split-gate GL-FET and PGL-FET with the structures schown schematically in Fig. 1. It is assumed that the gate voltages V_p and V_n have different signs, so that under gates the two-dimensional hole system (2DHS) and the two-dimensional electron system (2DES) are formed.

The developed device models for the GL-FET and PGL-FET detectors are based on the hydrodynamic equations governing the carrier transport in the 2DHS and 2DES in the gated regions and the Poisson equation for the self-consistent electric potential. They also describe the current-voltage characteristics of the lateral p-n junctions with uniform and perforated GLs determined by the thermionic carrier transport above and the tunneling transport under the barrier. The models include also equations which relate the ac voltages at the side contacts (and, hence, the rectified voltage component) and the intensity of the incident THz radiation.

In the framework of our model, the spatial distributions of $\delta\varphi_t^\pm(x)$ in the GL plane (along the axis x) are governed by the following system equations:

$$\frac{d^2\delta\varphi_\omega^+}{dx^2} + \frac{\omega(\omega + i\nu)}{s^2}\delta\varphi_\omega^+ = 0, \tag{1}$$

$$\frac{d^2\delta\varphi_\omega^-}{dx^2} + \frac{\omega(\omega + i\nu)}{s^2}\delta\varphi_\omega^- = 0. \tag{2}$$

Here ν is the collision frequency of holes and electrons in their channel sections, $s \geq \sqrt{\frac{4e^2W_g\varepsilon_F}{\kappa\hbar^2}} \propto \Sigma_0^{1/4}$ is the characteristic plasma-wave velocity in the gated GL structures, e is the
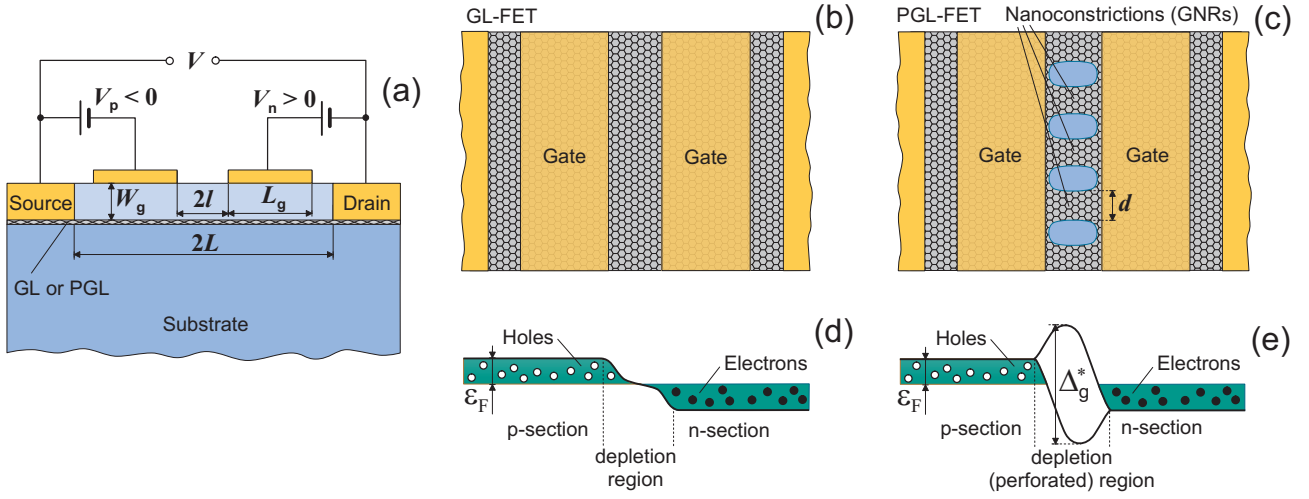
Fig. 1. Side and top views of GL-FET, (a) and (b), and PGL-FET, (a) and (c), and their band daigrams (d) and (e), respectively (at unbiased p-n junction).

electron charge, ε_F is the hole and electron Fermi energy in the gated sections, W_g and κ are the thickness and dielectric constant of the gate layer. The boundary conditions for Eqs. (1) and (2) given at the gate edges are as follows:

$$\delta\varphi_\omega^+|_{x=-L} = -\frac{\delta V_\omega}{2}, \qquad delta\varphi_\omega^-|_{x=L} = \frac{\delta V_\omega}{2}, \quad (3)$$

$$-\sigma_\omega \frac{d\,\delta\varphi_\omega^+}{dx}\bigg|_{x=-l} = \delta j_\omega^{pn}, \quad -\sigma_\omega \frac{d\,\delta\varphi_\omega^-}{dx}\bigg|_{x=l} = -\delta j_\omega^{pn}, \quad (4)$$

where $L \simeq L_g$ is the length of the p- and n- sections of the channel, L_g is the gate length, $2l$ is the spacing between the gates [see Fig. 1(a)], δj_ω^{pn} is the net ac current density in the p-n junction, which includes the displacement, tunneling, and thermionic components (determined by the geometrical capacitance, c^{pn}), of the p-n junction and its differential conductivity g^{pn} (calculated in [11]) and proportional to the ac voltage drop across the p-n junction). In Eqs. (1) and (2), we have omitted the nonlinear terms associated with the nonlinearity of the 2DES and 2DHS dynamics (in particular, the nonlinearity of the hydrodynamic equations for the 2DHS and 2DES), This is because, we focus on the GL-FET PGL-FET operation associated with another and stronger nonlinearity (nonlinearity of the p-n-junction current-voltage characteristics).

Equations (1) and (2) with boundary conditions (3) and (4) yield the following formulas for the spatial distributions of ac potentials $\delta\varphi_\omega^\pm$:

$$\delta\varphi_\omega^\pm = \mp\frac{\delta V_\omega}{2}\Bigg\{\cos[\text{æ}_\omega(x \pm L)]$$
$$+ \frac{\xi_\omega \sin(\text{æ}_\omega L_g) - \cos(\text{æ}_\omega L_g)}{\xi_\omega \cos(\text{æ}_\omega L_g) + \sin(\text{æ}_\omega L_g)} \sin[\text{æ}_\omega(x \pm L)]\Bigg\} \quad (5)$$

for the range $-L \leq x \leq -l$ for $\delta\varphi_\omega^+$, and $l \leq x \leq L$ for $\delta\varphi_\omega^-$. Here the wavenumber æ_ω and the characteristic plasma frequency for the gated 2DES and 2DHS Ω_g are given by

$$\text{æ}_\omega = \frac{\pi\sqrt{\omega(\omega + i\nu)}}{2\Omega_g L_g}, \quad \Omega_g = \frac{\pi s}{2L_g} = \sqrt{\frac{\pi e^2 \varepsilon_F}{4L_g^2 C\hbar^2}}. \quad (6)$$

The parameter $\xi_\omega = \sigma_\omega \text{æ}_\omega/[2g^{pn}(1 - i\omega\tau)]$, where σ_ω is the channel section dynamic conductivity and $\tau = c^{pn}/g^{pn}$ is the p-n junction recharging time, characterizes the ratio of the channel and p-n junction conductivities. The frequency dependence of ξ_ω is given by

$$\xi_\omega = i\sqrt{\frac{\omega}{\omega + i\nu}} \frac{\xi}{(1 - i\omega\tau)}, \quad (7)$$

where ξ is a function of the structural parameters (ξ is different for GL-FETS and GBL-FETs).

The voltage detector responsivity, R_ω, to the incoming THz radiation with the frequency ω is defined as

$$R_\omega = \overline{\Delta V}/SI_\omega. \quad (8)$$

Here $\overline{\Delta V}$ is the rectified dc voltage between the side contacts induced by the received signals, which is somewhat smaller than the rectified voltage component across the p-n junction $\overline{\Delta V}^{pn}$, hence, in the photovoltaic regime, $V_0 = \overline{\Delta V}$. The quantities $S = \lambda_\omega^2 G/4\pi$, I_ω and $\lambda_\omega = 2\pi c/\omega$ are the antenna aperture, the intensity of the incident THz radiation, and its wavelength, respectively, where c is the speed of light in vacuum and G is the antenna gain (we disregard its frequency dependence and put $G \sim 1.5$. The quantities $(\delta V_\omega)^2$ and I_ω are related to each other as $(\delta V_\omega)^2 = 4\lambda_\omega^2 I_\omega/\pi c$. The THz radiation coupling could be significantly improved using antennas optimized for such graphene structures.

The quantity $\overline{\Delta V}$ is proportional to $\overline{|\delta V_\omega^{pn}|^2}$, which, in turn, is determined by the spatial distributions of the ac potentials $\delta\varphi_\omega^\pm = \delta\varphi_\omega^\pm(x)$.

As follows from the our device models, the detector responsivity of both GL-FETs and PGL-FETs can be presented as:
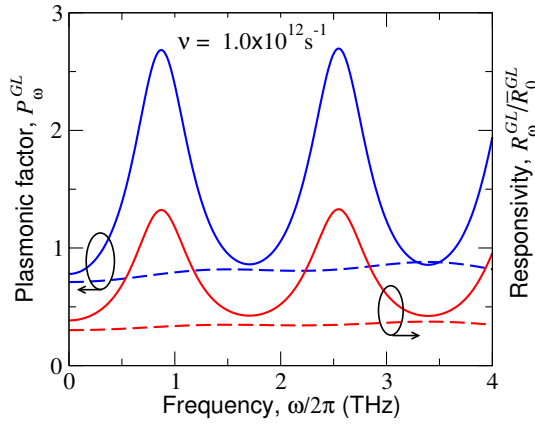
Fig. 2. Spectral dependences of the plasmonic factor P_ω^{GL} and the GL-FET responsivity $R_\omega^{GL}/\overline{R}_0^{GL}$ for $\nu = 1.0 \times 10^{12}$ s^{-1} and $L_g = 325$ nm. Other parameters are as follows: $l = 25$ nm, $W_g/\kappa = 1$ nm, and $\Omega_g/2\pi = 0.86$ THz- solid lines and $l = 10$ nm, $W_g/\kappa = 2.5$ nm, and $\Omega_g/2\pi = 1.17$ THz - dashed lines.

$$R_\omega^{GL} = \overline{R}_0^{GL} \cdot P_\omega^{GL}, \qquad R_\omega^{PGL} = \overline{R}_0^{PGL} \cdot P_\omega^{PGL}. \quad (9)$$

Here $\overline{R}_0^{GL}$ and $\overline{R}_0^{PGL}$ are the characteristic low-frequency responsivities and

$$P_\omega^{GL,PGL} = \left| \frac{\xi_\omega^{GL,PGL}}{\sin(\text{æ}_\omega L_g) + \xi_\omega^{GL,PGL} \cos(\text{æ}_\omega L_g)} \right|^2 \quad (10)$$

are the plasmonic factors, where æ_ω is the plasmonic oscillations wavenumber. The parameters ξ_ω^{GL} and ξ_ω^{PGL} characterize the ratio of the effective ac conductivity of the gated portions of the channel and the admittance of the p-n junction. Due to relatively low conductance of the PGL-FET p-n junction associated with the energy barrier in the constrictions leading to the tunneling transfer suppression, $|\xi_\omega^{GL}| \ll |\xi_\omega^{PGL}|$.

III. RESULTS

Using the developed PGL-FET device model, we calculated the spatial distributions of the potential, the ac and rectified currents, the dc voltage induced by the THz radiation between the side contacts, and the detector voltage responsivity R_ω^{PGL} as functions of the signal frequency ω, the gate voltages V_p and V_n, the geometrical parameters W_g, L, l, and d [see Fig. 1(a)], the hole and electron collision frequency ν, and the dielectric constant of the gate isolating layer κ.

Since the plasmonic factors P_ω^{GL} and P_ω^{PGL} exhibit oscillatory behavior as function of the frequency of incident THz radiation with the pronounced maxima at $\omega = (2n-1)\Omega_g$, where Ω_g is the plasmonic frequency and $n = 1, 2, 3, ...$ is the plasmonic resonance index, the detector responsivities R_ω^{GL} and R_ω^{PGL} can also exhibit a pronounced resonant maxima.

Figures 2–4 show examples the spectral characteristics of the plasmonic factor P_ω^{GL} and the GL-FET and PGL-FET detector resonsivities R_ω^{GL} and R_ω^{GL} calculated using the above equations for different parameters at room temperature.
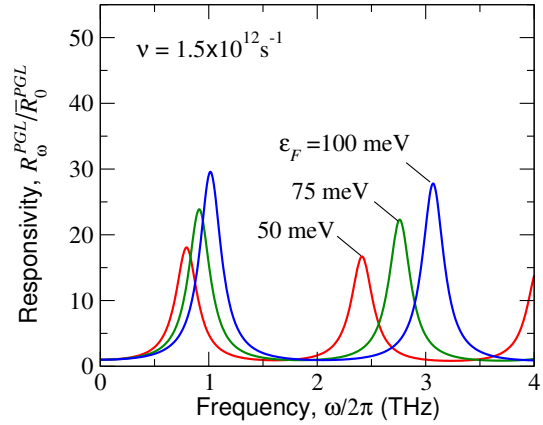
Fig. 3. Normalized PGL-FET resonsivity $R_\omega^{PGL}/\overline{R}_0^{PGL}$ versus frequency ω for different hole and electron Fermi energies ε_F ($\Delta_g = 200$ meV, $\nu = 1.5 \times 10^{12}$ s^{-1}, $L_g = 325$ nm, $W_g = 4$ nm, and $\kappa = 4$).
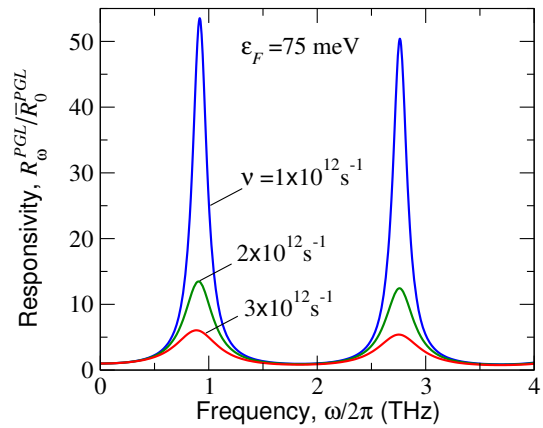
Fig. 4. The same as in Fig. 3 but for different ν and fixed ε_F.

One can see that the PGL-FETs exhibit much stronger resonant response due to substantially lower p-n junction conductance. Since the hole and electron Fermi energy ε_F increases with increasing gate voltages, a marked shift of the resonant peaks implies the possibility of the effective voltage control of the detector spectral characteristics. As seen from Fig. 4, an increase in the carrier collision frequency in the gated regions ν leads to s substantial drop of the plasmonic resonant peaks height, so that the GLs with a sufficiently high carrier mobility should be used, although the quality of the nanoconstrictions in the perforated region is less crucial.

IV. CONCLUSIONS

In summary, we proposed and evaluated resonant THz detectors (PGL-FET detectors) based on FETs with the split gates and electrically induced the lateral p-n junction. The gated regions of the GL- and PGL-FETs serve as the plasmonic resonant cavities. The p-n junction depletion PGL region provides the nonlinearity of the current-voltage characteristics. Using the developed device model, we calculated the spatial distributions of the ac and rectified components of electric potential and the thermionic and tunneling currents

induces by the incident THz radiation as well as the PGL-FET responsivity in the photovoltaic mode of operation. We showed that the responsivity can exhibit sharp maxima associated with the resonant excitation of plasmonic oscillations. The shape of the responsivity peaks, in particular their height, is dictated by the hole and electron collisions in the channel section and by the p-n junction depletion region conductance. Since due a suppression of the tunneling current in the PGL-FETs, the latter value in the PGL-FETs is much lower than in similar devices without the nanoconstrictions, the introduction of the latter result in a substantial improvement of the detector performance. The proposed PGL-FET devices can be effective resonant plasmonic THz detectors operating at room temperature.

ACKNOWLEDGMENT

REFERENCES

[1] V. V. Cheianov and V. I. Falko, "Selective transmission of Dirac electrons and ballistic magnetoresistance of np junctions in graphene," *Phys. Rev. B*, vol. 74, no. 4, pp. 041403-1–4, July 2006.

[2] A. Ossipov, M. Titov, and C. W. J. Beenakker, "Reentrance effect in a graphene npn junction coupled to a superconductor," *Phys. Rev. B*, vol. 75, no. 24, pp. 241401-1–4, June 2007.

[3] L. M. Zhang and M. M. Fogler, "Nonlinear Screening and Ballistic Transport in a Graphene pn Junction," *Phys. Rev. Lett.*, vol. 100, no. 1, pp. 116804-1–4, Mar. 2008.

[4] T. Low, S. Hong, J. Appenzeller, S. Datta, and M. S. Lundstrom, "Conductance asymmetry of graphene p-n junction," *IEEE Trans. Electron Devices*, vol. 56, no. 6, pp. 1292–1299, June 2009.

[5] M. I. Dyakonov and M. S. Shur, "Plasma wave electronics: novel terahertz devices using two dimensional electron fluid," *IEEE Trans. Electron Devices*, vol. 43, no. 10, pp. 1640–1645, Oct. 1996.

[6] S. A. Boubanga Tombet, Y. Tanimoto, A. Satou, T. Suemitsu, Y. Wang, H. Minamide, H. Ito, D. V. Fateev, V. V. Popov, and T. Otsuji, "Current driven detection of terahertz radiation in dual-grating-gate plasmonic detector," *Appl. Phys. Lett.*, vol. 104, no. 26, pp. 251114-1–4, July 2014.

[7] A. H. Castro Neto, F. Guinea, N. M. R. Peres, K. S. Novoselov, and A. K. Geim, "The electronic properties of graphene," *Rev. Mod. Phys.*, vol. 81, no. 1, pp. 109–162, Jan. 2009.

[8] L. Vicarelli, M. S. Vitiello, D. Coquillat, A. Lombardo, A. C. Ferrari, W. Knap, M. Polini, V. Pellegrini, and A. Tredicucci, "Graphene field-effect transistors as room-temperature terahertz detectors," *Nature Mat.*, vol. 11, pp. 865–871, Sep. 2012.

[9] X. Wang, Y. Quyang, X. Li, H. Wang, J. Guo, and H. Dai, "Room-temperature all-semiconducting sub-10-nm graphene nanoribbon field-effect transistors," *Phys. Rev. Lett.*, vol. 100, no. 20, pp. 206803-1–4, May 2008.

[10] G. S. Simin, M. Islam, M. Gaevski, R. Gashka, and M. S. Shur, "Low RC-constant perforated-channel HFET," *IEEE Electron Device Lett.*, vol. 35, no. 4, pp. 449–451, Feb. 2014.

[11] V. Ryzhii, M. Ryzhii, M. S. Shur, V. Mitin, A. Satou, and T. Otsuji, "Resonant plasmonic terahertz detection in graphene split-gate field-effect transistors with lateral pn junctions," *J. Phys. D: Appl. Phys.*, vol. 49, no. 31, pp. 315103-1-14, July 2016.